AGU100 ADVANCING EARTH AND SPACE SCIENCE

JGR

Journal of Geophysical Research: Biogeosciences

RESEARCH ARTICLE

10.1029/2018JG004441

Key Points:

- Concentrations of high solubility noble gases in a salt marsh pond are predicted well by wind speed-based gas exchange parameterizations
- However, ebullition must occur to explain concentrations of less soluble noble gases, and we infer ebullition rates from neon observations
- Including ebullition fluxes increased daily net oxygen production by 1–21%, making it an important oxygen flux in this setting

Supporting Information:

- Supporting Information S1

Correspondence to:
E. M. Howard,
ehoward@whoi.edu

Citation:
Howard, E. M., Forbrich, I., Giblin, A. E., Lott, D. E. III, Cahill, K. L., & Stanley, R. H. R. (2018). Using noble gases to compare parameterizations of air-water gas exchange and to constrain oxygen losses by ebullition in a shallow aquatic environment. *Journal of Geophysical Research: Biogeosciences*, *123*, 2711–2726. https://doi.org/10.1029/2018JG004441

Received 9 FEB 2018
Accepted 23 JUL 2018
Accepted article online 30 JUL 2018
Published online 7 SEP 2018

Using Noble Gases to Compare Parameterizations of Air-Water Gas Exchange and to Constrain Oxygen Losses by Ebullition in a Shallow Aquatic Environment

Evan M. Howard[1,2], Inke Forbrich[3], Anne E. Giblin[3], Dempsey E. Lott III[4], Kevin L. Cahill[4], and Rachel H. R. Stanley[5]

[1]University of Washington School of Oceanography, Seattle, WA, USA, [2]Massachusetts Institute of Technology/Woods Hole Oceanographic Institution Joint Program in Oceanography/Applied Ocean Science and Engineering, Woods Hole, MA, USA, [3]The Ecosystems Center, Marine Biological Laboratory, University of Chicago, Woods Hole, MA, USA, [4]Department of Marine Chemistry and Geochemistry, Woods Hole Oceanographic Institution, Woods Hole, MA, USA, [5]Department of Chemistry, Wellesley College, Wellesley, MA, USA

Abstract Accurate determination of air-water gas exchange fluxes is critically important for calculating ecosystem metabolism rates from dissolved oxygen in shallow aquatic environments. We present a unique data set of the noble gases neon, argon, krypton, and xenon in a salt marsh pond to demonstrate how the dissolved noble gases can be used to quantify gas transfer processes and evaluate gas exchange parameterizations in shallow, near-shore environments. These noble gases are sensitive to a variety of physical processes, including bubbling. We thus additionally use this data set to demonstrate how dissolved noble gases can be used to assess the contribution of bubbling from the sediments (ebullition) to gas fluxes. We find that while literature gas exchange parameterizations do well in modeling more soluble gases, ebullition must be accounted for in order to correctly calculate fluxes of the lighter noble gases. In particular, for neon and argon, the ebullition flux is larger than the differences in the diffusive gas exchange flux estimated by four different wind speed-based parameterizations for gas exchange. We present an application of noble gas derived ebullition rates to improve estimates of oxygen metabolic fluxes in this shallow pond environment. Up to 21% of daily net oxygen production by photosynthesis may be lost from the pond via ebullition during some periods of biologically and physically produced supersaturation. Ebullition could be an important flux of oxygen and other gases that is measurable with noble gases in other shallow aquatic environments.

1. Introduction

Shallow aquatic environments such as estuaries and lakes vary widely in biological productivity and have dynamic diel cycles of oxygen (O_2) influx and efflux. Measurements of O_2 are often paired with parameterizations of diffusive gas exchange based on wind speed to calculate net ecosystem metabolic fluxes (equivalently, net community production; Caffrey 2004, Staehr et al., 2010). While an accurate estimate of air-water gas exchange fluxes is critical to determining these metabolic fluxes, these estimates may be poorly constrained because existing gas exchange parameterizations for coastal and inland waters often lack fundamental mechanisms of gas transfer in shallow environments (Zappa et al., 2007).

These mechanisms include bubble processes, turbulence generated from bottom stress or buoyancy fluxes, and fetch limitation of wind-driven turbulence (Crosswell, 2015; MacIntyre et al., 2010; Vachon & Prairie, 2013). A further limitation of many existing gas exchange parameterizations in these settings is that they are derived using the efflux of a single gas such as sulfur hexafluoride, carbon dioxide (CO_2), or methane (CH_4) (Cole et al., 2010). Relationships between efflux processes and gas exchange may not be readily applicable to the range of influx processes for these gases. Most importantly, these gases have very different sensitivities to air injection (bubbles added by breaking waves) and ebullition (the formation and rise of bubbles from the sediments) than O_2 and other gases of intermediate solubility—making gas exchange parameterizations from any single tracer difficult to scale to other gases of interest. Direct measurements of ebullition are challenging (e.g. Delwiche & Hemond, 2017a) and typically cannot yet be parameterized. However, ebullition has been measured to be a major gas efflux pathway relative to diffusive exchange in some shallow aquatic settings for biologically generated gases including nitrogen (N_2; ebullition flux in a pond similar to

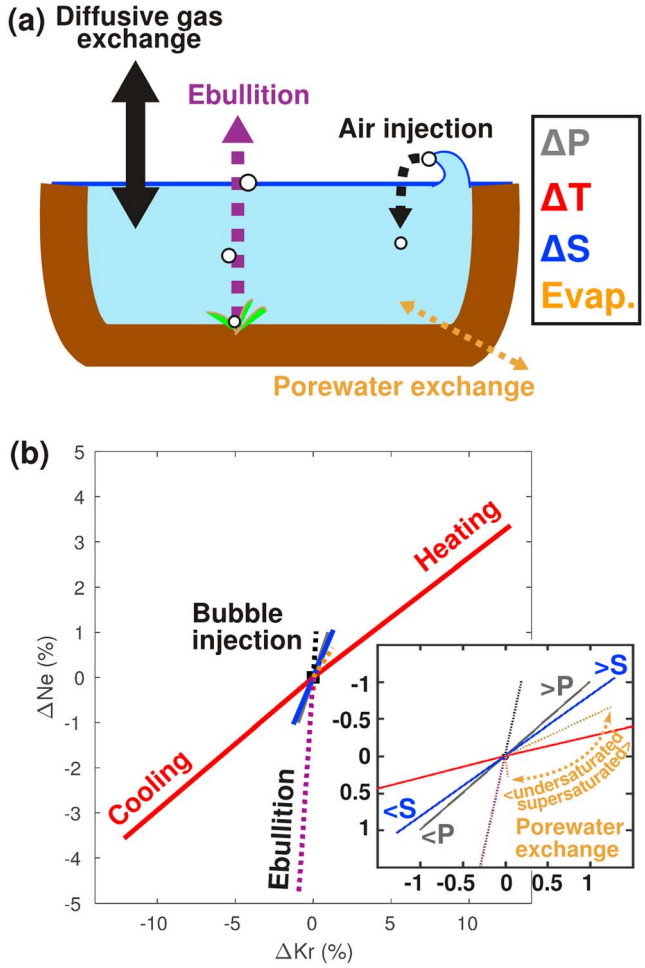

Figure 1. Processes that can change noble gas saturation state relative to atmospheric equilibrium in a tidally isolated salt marsh pond. A conceptual diagram of the pond (a): dissolved gas fluxes are identified with arrows, including diffusive gas exchange, ebullition from biologically generated bubbles, air (bubble) injection from breaking waves, and exchange with adjacent porewater. Other environmental parameters that change the saturation state of dissolved gases (boxed to the right of the diagram) include changes in atmospheric pressure, water temperature, and salinity (*P*, *T*, and *S*) and evaporation of pond water (same slope as *P* line but smaller magnitude). The effects of these processes and parameters on the saturation state of neon (ΔNe, a less soluble gas) and krypton (ΔKr, a more soluble gas) are plotted (b) relative to initial conditions at saturation with respect to the atmosphere (T = 27 °C, S = 30 on practical salinity scale of 1978, P = 1 atm). Diffusive gas exchange drives ΔNe and ΔKr toward 0% (saturation). Effects of properties that are well constrained by measured environmental variables are identified with solid lines, and their length reflects the change in saturation state expected for an instantaneous change in that property over the range of pond observations, without other any exchange processes. The length of dashed lines indicate upper bounds to the effects of poorly constrained processes in the study pond based on literature parameterizations of these processes in other settings—the actual magnitudes of these processes in the pond will depend on in situ conditions during the sampling periods and are likely to be smaller than these upper bounds (see supporting information Text S2). Porewater exchange may affect dissolved gases differently depending on the porewater composition (modeled as T = 12 °C, the approximate annual mean porewater temperature, S = 25 on practical salinity scale of 1978, and between 30% undersaturated and 30% supersaturated).

diffusive fluxes in other settings; Gao et al., 2013), CH_4 and CO_2 (ebullition 95–97% of CH_4 and 13–35% of CO_2 net fluxes in a rice paddy; Komiya et al., 2015), and O_2 (10–22% of net fluxes in a lake and reservoir; Koschorreck et al., 2017).

The result of these limitations is that gas exchange parameterizations may be site specific and fluxes predicted using different parameterizations can range over an order of magnitude (Borges et al., 2004; Kremer et al., 2003). Determination of gas exchange fluxes is thus often the largest source of error in estimates of metabolic rates from open water O_2 measurements.

The noble gases neon (Ne), argon (Ar), krypton (Kr), and xenon (Xe) are a suite of naturally occurring, biologically inert tracers that vary widely in solubility and are sensitive to a range of physical processes. For example, more soluble gases including Kr and Xe are very sensitive to changes in temperature, while less soluble Ne is highly sensitive to bubble processes because insoluble gases preferentially partition into the gas phase when bubbles are present. Ar exhibits intermediate sensitivity to these processes and behaves much like O_2 due to a similarity in physicochemical characteristics between the two gases. Processes and environmental changes that may affect gas concentrations and saturation states in a shallow, tidally isolated aquatic setting are plotted in Figure 1a, and the resulting potential effects on Ne and Kr in this study are plotted as changes in saturation state (Figure 1b) relative to solubility equilibrium concentrations, that is, $\Delta Ne = ([Ne]/[Ne]_{sat} - 1) * 100\%$. These processes and parameters include diffusive gas exchange, changes in temperature, salinity, and atmospheric pressure, as well as bubble processes in the water column (Bieri, 1971; Hamme et al., 2017; Stanley & Jenkins, 2013). Additionally, noble gases partition between porewater and bubbles in sediment (e.g. Aeschbach-Hertig et al., 2008; Stute & Scholsser, 1993), and disequilibria of noble gases in sediment porewater have been used to diagnose ebullition (Brennwald et al., 2005). This mechanism should also affect noble gas saturation states in the water column and bubbles during ebullition.

In this study, we analyze a unique data set of Ne, Ar, Kr, and Xe and highlight a new technique for measuring of the effects of ebullition on dissolved gas fluxes. First, we evaluate how four commonly used gas exchange parameterizations perform in predicting gas concentrations in a salt marsh pond. Three of these parameterizations are derived from studies in analogous freshwater environments, lakes and ponds (Cole & Caraco, 1998; Crusius & Wanninkhof, 2003; Vachon & Prairie, 2013), and the fourth from ocean data (Wanninkhof, 2014). Shallow (<0.5 m deep) marine ponds are abundant and dynamic features of temperate salt marshes (Spivak et al., 2017; Wilson et al., 2014). Gas exchange parameterizations specific to such environments have not been experimentally determined, and picking an appropriate parameterization is critical for the determination of metabolic fluxes in such settings.

We find that the observations of the more soluble noble gases in this study are well described by standard gas exchange parameterizations, but the behavior of less soluble noble gases are not. Therefore we evaluate the contribution of ebullition to air-water fluxes of dissolved gases. We conclude by estimating how much photosynthetic O_2 might be removed from the pond by ebullition and the resulting effect on metabolic rates calculated from an oxygen mass balance, in order to highlight a potential application of this technique.

Table 1
Environmental Variability During Sample Period, and Expected Maximum Effects on Noble Gas Saturation States Relative to Atmospheric Equilibrium by Parameters That Change Saturation Concentration and by Processes That Add or Remove Dissolved Gas

Environmental parameters	Mean (std. dev.) [range]		ΔNe (%)	ΔKr (%)
	Study period: 29 Jul (6:00–19:00)			
Temperature (°C)	24.5 (2.8)	[20.4 to 27.7]	4.6	17.1
Salinity[a]	27.9 (0.2)	[27.7 to 28.3]	0.3	0.4
ΔO_2 (%)[b]	1 (33)	[−56 to 41]		
U_{10} (m s^{-1})[c]	4.4 (1.5)	[1.6 to 6.5]		
PAR (mmol m^{-2} s^{-1})[d]	0.96 (0.60)	[0.04 to 1.75]		
Atmospheric pressure (kPa)	100.769 (0.184)	[100.410 to 101.105]	0.7	0.7
	Study period: 25 Aug (20:30–00:45)			
Temperature (°C)	26.3 (0.8)	[25.2 to 27.7]	1.4	5.3
Salinity	32.0 (0.1)	[31.8 to 32.2]	0.2	0.3
ΔO_2 (%)	−42 (16)	[−63 to −10]		
U_{10} (m s^{-1})	1.6 (0.6)	[0.9 to 2.7]		
PAR (mmol m^{-2} s^{-1})	0.00 (0.00)	[0.00 to 0.00]		
Atmospheric pressure (kPa)	101.910 (0.015)	[101.892 to 101.934]	<0.1	<0.1
	Study period: 26 Aug (9:15–15:45)			
Temperature (°C)	28.8 (2.4)	[24.0 to 31.2]	4.1	15.8
Salinity	32.1 (0.2)	[31.8 to 32.4]	0.3	0.4
ΔO_2 (%)	15 (32)	[−51 to 50]		
U_{10} (m s^{-1})	3.9 (1.4)	[1.5 to 5.7]		
PAR (mmol m^{-2} s^{-1})	1.30 (0.31)	[0.54 to 1.61]		
Atmospheric pressure (kPa)	101.838 (0.114)	[101.634 to 101.997]	0.4	0.4
	Processes (add or remove dissolved gas)			
Ebullition[e]			~5	~1
Porewater exchange[f]			<0.7	<1.2

[a]Practical salinity scale of 1978, unitless. [b]Saturation state relative to solubility equilibrium of gas, as defined in text. [c]Wind speed at 10 m, stability corrected using log wind profile, as defined in text. [d]Photosynthetically active radiation at 400–700-nm wavelengths. [e]Estimated from lower-bound (equilibrium bubble composition) effect of rates in Cheng et al. (2014). [f]Estimated for upper bound of tidally variant porewater exchange rates and gases within 30% of atmospheric equilibrium with annual average groundwater temperature using the model of Nuttle and Hemond (1988; see supporting information Text S2).

2. Methods

2.1. Setting and Sampling Methods

The study location was a salt marsh pond in the Plum Island Ecosystems Long Term Ecological Research site in Massachusetts, USA (42.7411°N, 70.8309°W), and has been previously described in Spivak et al. (2017, 2018). The pond was circular, covered 7,000 m^2, and had 25 cm mean depth during the study period. Five to ten meters of grass-covered high marsh separated the pond from an adjacent tidal creek. Water from the creek flooded the pond during spring tides every two weeks. In summer 2014, three sub-daily sampling periods were sampled when the pond was tidally isolated from the adjacent creek, including two daytime periods and one nighttime period. Table 1 presents the variability in environmental conditions over the sampling periods, as well as the expected maximum change in noble gas saturation state if either (1) a given parameter was rapidly increased across the range of observed values without intermediate equilibration or (2) a process was sustained at constant rate derived from a literature parameterization over the entire sampling period without other environmental changes. The mean saturation concentrations expected at atmospheric equilibrium for each of the noble gases over each experimental period are also summarized in the supporting information, Table S1.

Temperature, salinity (calculated from conductivity), and O_2 saturation state data were collected every 15 min using a YSI™ Exo2 water quality sonde located near the center of the pond. The sonde was calibrated before and after each sampling period using a one-point calibration to water-saturated air for O_2 (zero-O_2 calibration was performed in May 2014) and a two-point calibration of the conductivity cell (YSI™ conductivity standards of 1×10^4 and 5×10^4 μS cm^{-1}). Wind speed at 4.16 m height, atmospheric pressure, and meteorological measurements used to calculate the wind speed at 10 m height (U_{10}) were determined using a

meteorological tower located roughly 200 m from the study pond (Forbrich & Giblin, 2015). U_{10} was calculated using the stability-corrected log wind profile (Walmsley, 1988) corrected for displacement of the zero-wind level by ground obstructions (~5 cm) and the roughness length scale of grasses on the high marsh (~1 cm) (e.g. Tsai & Tsuang, 2005).

Dissolved noble gases were sampled using crimped copper tube sampling (Jenkins et al., 2010), with the modification that water samples were hand-pumped through the copper tube using presoaked plastic tubing extended ~1 m away from the pond bank (10 m from the sonde). Sample frequency varied from 2 to 4 h over the three sampling periods, and two-pairs of duplicates were sampled on 29 July 2014 (at roughly 0900 and 1600 h). Gases were extracted and concentrations of noble gases determined on a quadrupole mass spectrometer (Stanley, Baschek, et al., 2009); Ne and Ar were determined using peak height manometry and Kr and Xe using ratiometric isotope dilution.

Uncertainties in the noble gas concentrations were calculated from the mean coefficient of variation from duplicate samples and were similar to analytical uncertainties reported by the WHOI Isotope Geochemistry Facility. Saturation state uncertainties were calculated using the mean coefficient of variation from a Monte Carlo approach, in which measured concentration uncertainties as well as temperature and salinity (the dominant sources of uncertainty in the saturation concentration) were allowed to randomly vary within the observed variability from a spatial survey of the pond (standard deviation of 1 °C, 0.5 standard deviation in salinity on the practical salinity scale of 1978) over 3,000 iterations. Data and uncertainties for the noble gases and environmental data are accessible as described in the Acknowledgements and Data Availability statement.

2.2. Gas Exchange Model Evaluations

The gas exchange parameterizations evaluated in this study were chosen because they are representative of pond, lake, or ocean environments where enhanced mixing by tidal currents is not a major source of gas exchange, are functions of readily measureable environmental parameters such as wind speed, and have been applied in other studies as well as modeling toolboxes (Winslow et al., 2016). Each parameterization was originally derived following the form:

$$\frac{dC}{dt} * z * \rho = k_C * (C_{sat} - C) * \rho \tag{1}$$

where z is the water depth (m), C is the concentration of a given gas (μmol kg^{-1}), C_{sat} is the temperature, salinity, and pressure dependent saturation concentration of that gas, and ρ is the density (kg m^{-3}) to convert concentrations to volumetric units. k_C is the gas transfer velocity (m h^{-1}), and is scaled between gases using the Schmidt number (Sc, the unitless ratio of kinematic viscosity of water to molecular diffusivity of the gas):

$$\frac{k_a}{k_b} = \left(\frac{Sc_a}{Sc_b}\right)^{-0.5} \tag{2}$$

where the subscripts represent two gases and the exponent of −0.5 is appropriate for a non-smooth water surface (ripples or small waves were always observed; nonetheless, using a coefficient of −0.67 for a smooth surface lacking capillary ripples, or an intermediate, variable coefficient, did not qualitatively change any of the results discussed in this work). k_C is often scaled to that of CO_2 at 20 °C (Sc = 600, in freshwater), reported as k_{600} (cm h^{-1}).

The parameterizations evaluated in this study are scaled to k_{600} and reproduced here:

Wanninkhof (2014), equation (4): $$k_{600} = 0.24(0.05) * {U_{10}}^2 \tag{3}$$

Cole and Caraco (1998), equation (5): $$k_{600} = 2.07 + 2.15 * {U_{10}}^{1.7} \tag{4}$$

Crusius and Wanninkhof (2003), $$k_{600} = 0.72(0.36) * U_{10} \quad \left[U_{10} < 3.7 \text{ m s}^{-1}\right] \tag{5a}$$

Equations (5) and (6): $$k_{600} = -13.3(27.1) + 4.33(5.31) * U_{10} \left[U_{10} > 3.7 \text{ m s}^{-1}\right] \tag{5b}$$

Vachon and Prairie (2003), Table 2, equation (B): $$k_{600} = 2.51(0.99) + 1.48(0.34) * U_{10} + 0.39(0.08) * U_{10} * SA. \tag{6}$$

Table 2
Root Mean Square Error (RMSE) for Model Evaluations of Saturation State (% Deviation From Atmospheric Equilibrium) With Each Gas Exchange Parameterization (Duplicate Samples Averaged)

RMSE of	Wanninkhof (2014)	Cole and Caraco (1998)	Crusius and Wanninkhof (2003)	Vachon and Prairie (2013)
(n = 4)		*Study period: 19 Jul (6:00–19:00)*		
Ne	2.5	2.8	2.4	2.4
Ar	3.0	2.8	2.8	2.4
Kr	1.8	1.8	1.7	1.5
Xe	2.3	2.1	2.3	2.0
(n=3[a])		*Study period: 25 Aug (20:30–00:45)*		
Ne	2.8	2.5	2.7	2.4
Ar	1.6	1.0	1.4	1.0
Kr	1.3	1.0	1.2	0.9
Xe	1.2	0.8	1.1	0.8
(n = 3)		*Study period: 26 Aug (9:15–15:45)*		
Ne	1.4	1.8	1.3	1.3
Ar	2.9	3.9	2.7	3.1
Kr	1.9	3.1	1.6	1.9
Xe	3.5	2.1	4.0	3.4
(n = 10[a])		*Pooled data from all three periods*		
Ne	2.3	2.4	2.2	2.1
Ar	2.7	3.0	2.5	2.4
Kr	1.7	2.1	1.5	1.5
Xe	2.5	1.8	2.7	2.3
All gases	2.5	2.3	2.3	1.9

[a]n = 2 (25 August) or n = 9 (pooled data) for Ne and Ar, nighttime sample with likely contamination excluded.

Standard deviations for the parameterization terms are in parentheses (where assessable from the original publications). In equation (6), *SA* is the surface area (km^2) of the water body; this acts to integrate the effects of fetch. Nonzero intercepts (gas exchange in the absence of wind) in equations (4) and (6) are empirical fits for nonwind sources of turbulence, such as buoyancy fluxes.

Each parameterization was evaluated by initializing a bulk water model with the measured concentrations of Ne, Ar, Kr, and Xe, and the temperature, salinity, and pressure dependent saturation concentrations, and running the discretized form of equation (1) forward at 15 min intervals using k_C predicted for each gas (equations (2)–(6)). For example, for each step i of time Δt, the concentration for the subsequent C_{i+1} is modeled as follows:

$$C_{i+1} = k_{C,i} * \left(C_{\mathrm{sat},i} - C_i\right) * \Delta t / z + C_i \tag{7}$$

The saturation concentration and saturation state of each gas ($\Delta C = [C/C_{\mathrm{sat}} - 1] * 100\%$) was determined using recent solubility functions (performed by D. E. Lott III and W. J. Jenkins at the WHOI Isotope Geochemistry Facility as described at www.whoi.edu/sites/IGF/). Mean saturation concentrations of each gas from the Lott and Jenkins solubility functions are summarized in Table S1, and saturation concentrations are listed with each measurement with the original data, accessible as described in the data availability statement.

The resulting saturation concentrations expected at atmospheric equilibrium lead to slightly lower saturation states for Ne, Kr, and Xe for our samples than previously published solubilities (Hamme & Emerson, 2004; Weiss & Kyser, 1978; Wood & Caputi, 1966). We chose the more recent solubility functions because all noble gas solubilities were measured from the same samples on the same instrument, which was also the instrument used to analyze the samples in this study. Thus using these solubility functions as a set is more internally consistent than using a set of solubilities measured at different laboratories (Manning, Stanley, Nicholson, et al., 2016). In practice this choice does not qualitatively change most results discussed in this work. Results derived from either the new or previously published solubility functions are compared in the supporting information (Text S1).

The modeled gas saturation states were compared to those of the samples at equivalent points in time by calculating the root mean square error (RMSE) over each sampling period and over the entire study period.

2.3. Calculating Ebullition Rates and Resulting Fluxes Using Neon

By incorporating an additional term for ebullition, the mass balance of a bubble-sensitive gas such as Ne can be used to calculate the product of the total ebullition rate, E (mL bubbles m^{-2} h^{-1}), and the concentration of that gas in escaping bubbles, C_b (μmol mL^{-1} bubble):

$$\frac{dC}{dt} * z * \rho = k_C * (C_{sat} - C) * \rho - (E * C_b + \varepsilon) \tag{8}$$

$$E * C_b + \varepsilon = -\rho * \left[\frac{dC}{dt} * z - k_C * (C_{sat} - C)\right] \tag{9}$$

ε represents errors or other terms in the mass balance that are not parameterized in equation (8). Equation (9) rearranges the mass balance in equation (8) to solve for the gas-specific ebullition flux (E * C_b, including unconstrained errors) in terms of the known gas concentrations. E and C_b can vary inversely, so the magnitudes of the two terms are not separately known without some constraint on C_b of the gas of interest. C_b depends on the bubble size (and thus rate of rise) and gas transfer between the bubble and surrounding water (Keeling, 1993; Merlivat & Memery, 1983). In order to solve equation (9) for E, C_b was calculated using empirical and theoretical relationships relating water-bubble gas transfer (Nock et al., 2016) to the bubble-size dependent rise rate (Park et al., 2017) over a range of bubble sizes and initial bubble gas composition (in our case enrichment in O_2). In this setting, kinetic limitation on gas transfer controls C_b when bubbles are both larger than 0.5 mm diameter and have initial concentrations far from equilibrium with the surrounding water (e.g. a pure oxygen bubble). Further details of the kinetic bubble model used in this calculation are provided in the supporting information (Text S4 and Figure S5).

The model framework used to evaluate the gas exchange parameterizations in equations (3) through (6) was expanded to include equations (8) and (9) in order to calculate the Ne-specific ebullition flux at each model step in time. In order to determine E while minimizing overfitting of ε, we performed a constrained, tapered least squares optimization (Wunsch, 2006); only positive E was allowed, and values of E and modeled concentrations C (evaluated at 15 min increments) were optimized so as to minimize misfit with measured concentrations (5–7 samples) while selecting for smoothly varying model C and E time series. Additional details of the optimization method are provided in the supporting information. Using E determined from Ne, equation (8) was then solved for each of the noble gases, and the modeled results including ebullition fluxes compared to those from diffusive gas exchange only.

3. Results and Discussion

3.1. Gas Exchange Model Results

Measured and modeled noble gas saturation states are plotted in Figure 2. Uncertainties in sample saturation state were dominated by uncertainties in the pond's temperature; observed spatial heterogeneity was up to 1 °C during spatial surveys around the pond over the same times of day (but different days than those sampled). Modeled values of ΔKr and ΔXe, the most soluble of the four gases, generally agreed well with sampled saturation state, though the initial rise of ΔXe was underestimated by the model evaluations on the morning of 26 August. In contrast, ΔAr and especially ΔNe tended to be lower than model predictions during the day. As the pond cooled at night, ΔNe and ΔAr were in better agreement with modeled values, excluding a single sample that had a pattern of supersaturation for Ne and Ar characteristic of sample contamination by a small air bubble (the effect of such contamination on Kr and Xe was negligible because of their greater solubility).

The model evaluations with the best agreement to measurements of each gas varied by sampling period, but in general, the parameterization from Vachon and Prairie (2013) resulted in low RMSE fits to the data (Table 2). Over the entire study, this parameterization led to the best agreement to the pooled data for all gases and for Ne, Ar, and Kr separately. Cole and Caraco (1998) led to the best overall agreement for Xe.

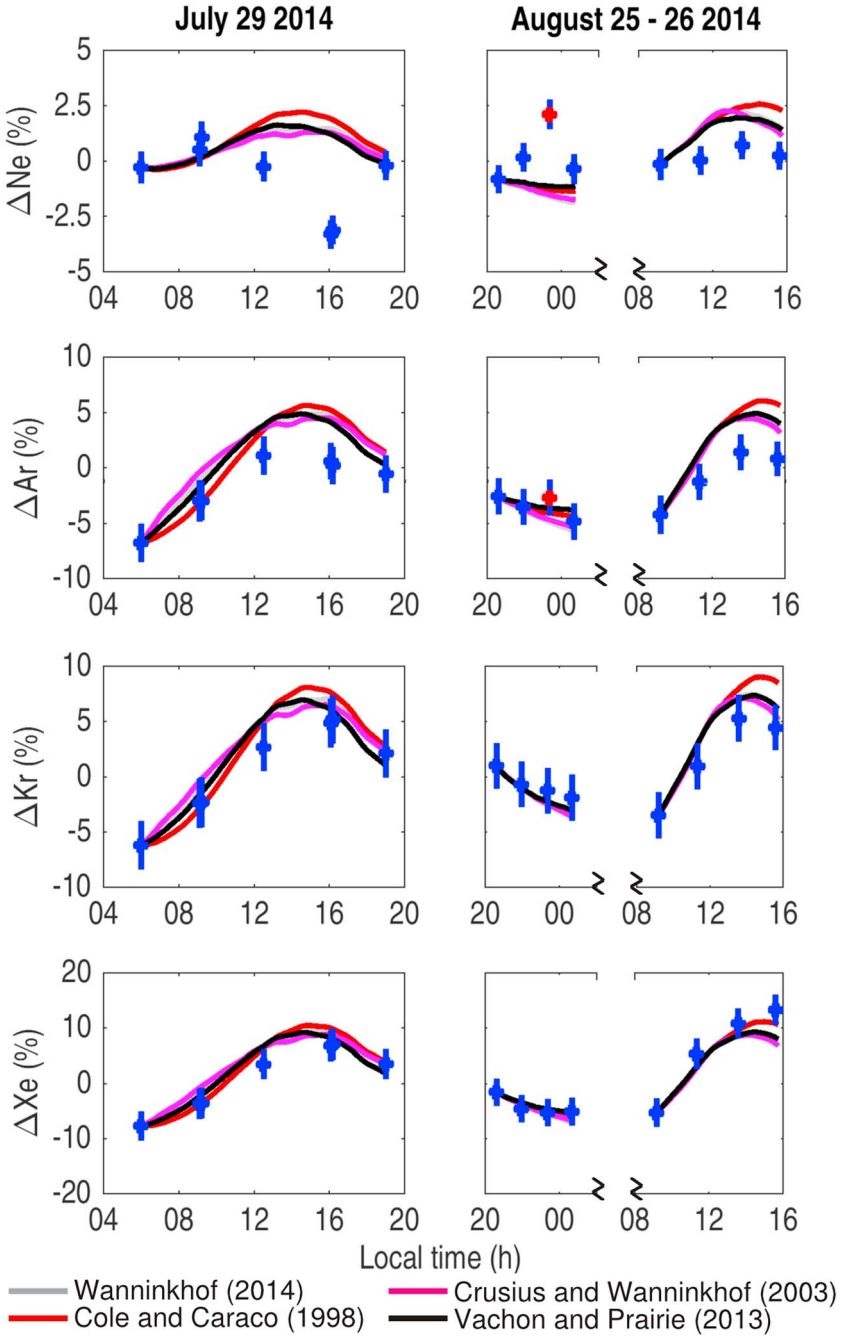

Figure 2. Saturation states of neon (ΔNe), argon (ΔAr), krypton (ΔKr), and xenon (ΔXe) in blue circles (with one standard deviation error bars) for the three study periods, relative to in situ saturation concentrations corrected for changes in atmospheric pressure. Modeled saturation states are plotted as lines based on initial conditions and the gas exchange parameterizations from Wanninkhof (2014; gray), Cole and Caraco (1998; red), Crusius and Wanninkhof (2003; purple), and Vachon and Prairie, (2013; black). On the night of 25 August, measurements of Ne and Ar from one sample (red circle) were likely contaminated by an air bubble during sampling (see text).

3.2. Interpreting Noble Gas Signals

The strong model agreement to measured ΔKr and ΔXe, high solubility gases for which bubble processes are expected to be unimportant, indicates that the models based on all four wind speed based parameterizations performed well in describing diffusive gas exchange in this setting. However, a notable feature of the data set

was the low ΔNe and ΔAr during some daytime points compared to that expected from the diffusive gas exchange; this offset was larger than the difference between the parameterizations. Changes in environmental parameters including temperature, salinity, and atmospheric pressure identically affected the saturation concentrations expected at atmospheric equilibrium for measured and modeled gases and cannot explain this offset.

Decreasing saturation concentrations, driven largely by daytime warming of the pond, mean that the noble gas saturation states should increase until rising supersaturation is compensated by a larger air-water gradient and enhanced gas exchange (equation (1)). This expected behavior was observed in ΔKr and ΔXe. Measured concentrations and saturation states deviated from atmospheric equilibrium because temperature changes were rapid relative to the gas exchange timescale (measured concentrations for the noble gases, as well as O_2 are plotted against saturation concentrations in Figure S4). However, measured ΔNe and ΔAr either decreased, or increased more slowly than expected given the gas transfer velocity.

Other processes identified as potential drivers of changing saturation state in the pond (Figure 1) were evaluated, but a number were determined to have small effects on the observations over the sampling periods compared to the observed signals. Potential effects of evaporation (Linacre, 1993), porewater exchange (Nuttle & Hemond, 1988), and air injection (Stanley, Jenkins, et al., 2009) are evaluated in the supporting information and were expected to cause ~1% or less relative difference in saturation state for all gases. None of these processes were thus expected to result in the observed variability; however, they may be important and detectable using noble gases at other times in the pond and in other environments such as nearby tidal creeks (Howard, 2017).

There was a small increase in nighttime ΔNe compared to the model evaluations that was not readily explained by the evaluated processes. ΔNe was close to 0%, while the wind speed based parameterizations predicted gas exchange that was too slow relative to decreasing pond temperature to keep the water at equilibrium. Ne values close to saturation could imply that there was an additional nighttime source of mixing, for example enhanced nighttime convection (MacIntyre et al., 2010; Read et al., 2012). While we could not explicitly test parameterizations of these processes for our nighttime study period (vertical water temperature gradients were not evaluated at night), gas exchange parameterizations including convective overturn have been shown to increase nighttime k_C by a factor of two or more compared to wind speed based parameterizations in a small lake of similar area (but 8 m depth; Dugan et al., 2016). Such an increase with respect to Ne would drive it to atmospheric equilibrium at night but is not sufficient to drive more soluble and slower diffusing Xe and Kr all the way to equilibrium.

The same processes cannot, however, explain the larger measured disequilibrium of Ne compared to the model predictions in the daytime sampling periods; daytime k_C differences between wind speed based parameterizations and those including additional convective components are much smaller in general (Dugan et al., 2016). Also, despite the horizontal temperature heterogeneity related to semi-isolated side basins of the pond, we observed no midday vertical temperature gradients within the pond—it appeared to be well mixed vertically as would be expected for such a shallow (25 cm) body of water with wind-driven waves. Using a greater k_C than predicted by the gas exchange parameterizations or than is inferred from the Xe and Kr mass balances (supporting information, Table S2) could improve the fit of Ar and Ne to some extent (while worsening the fit of Xe) but would not be sufficient to explain the lower Ne relative to the other gases.

Ebullition is the remaining and most plausible explanation for observed differences between measured and modeled saturation states of the lighter noble gases. Indeed, pronounced daytime decreases in ΔNe and ΔAr on 29 July were characteristic of the expected effects of ebullition since diffusive gas exchange alone is sufficient to explain ΔKr and ΔXe and ebullition removes less soluble gases preferentially; more soluble gases are expected to predominantly remain dissolved in the surrounding water. Supporting this idea, we observed abundant bubbles rising from the pond bottom both from the surface of and in the vicinity of benthic macroalgae during daytime periods (Figure 3). Ebullition of O_2 and CH_4 enriched bubbles in other shallow marine sediments (Cheng et al., 2014) can be sufficiently large to explain such decreases in ΔNe and ΔAr (Figure 1b**,** Table 1), with high spatial and temporal variability; similar variability in ebullition may explain the larger differences between modeled and measured ΔNe and ΔAr on 29 July than on 26 August.

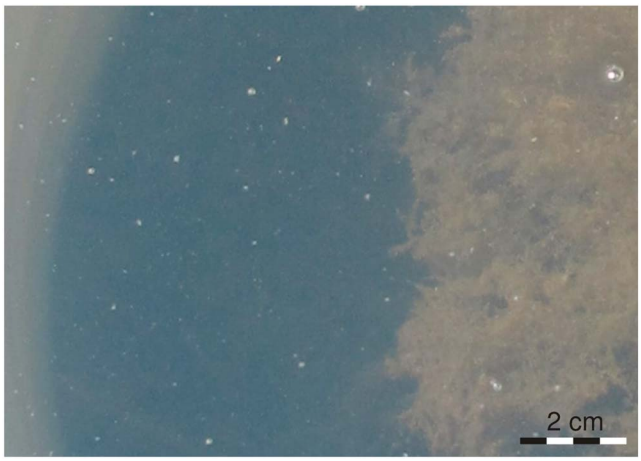

Figure 3. Bubbles rising from macroalgae on the pond bottom, viewed from roughly 10 cm above the water surface over shaded and unshaded areas. (Photograph taken by Chawalit Charoenpong)

3.3. Ebullition Model Results

The four gas exchange parameterizations we evaluated did well in explaining observed changes in Kr and Xe, and ebullition could theoretically explain most of the difference between modeled and observed values of Ne and Ar. Therefore we combined our observations of Ne concentrations with the gas exchange parameterization-based models to constrain ebullition. Bubbles that form on the pond bottom break free and rise to the water surface because of increasing buoyancy with size, physical disturbances, or transient decreases in pressure (e.g. from wave troughs; Maeck et al., 2014). Not all bubbles formed in the pond will rise to the surface (some remain at nucleation points, dissolve, or become trapped under vegetation), but those that ultimately escape contribute to disequilibrium of Ne and Ar between the pond and atmosphere. These bubbles gain Ne, Ar, and other gases by diffusion from the surrounding pond water. If the bubbles are relatively small (less than ~0.5 cm in diameter) and take more than tens of seconds to escape the pond after their initial formation, then the gas concentrations in the bubbles are expected to approach equilibrium with the surrounding water (based on water-bubble gas-specific transfer velocities on the order of 10^{-5} to 10^{-4} m s^{-1} calculated using the parameterizations of Nock et al., 2016; details in supporting information Text S4).

We calculated the ebullition rate E derived from Ne concentrations using a constrained optimized solution for equation (8). We infer that ebullition is driven by photosynthesis in this setting (see section 3.4), rather than methanogenesis. Methanogenesis should be strongly limited by high rates of sulfate reduction that occur in this pond (Spivak et al., 2018). Therefore E was evaluated over a large range of possible bubble sizes and initial enrichment of O_2; these parameters control the initial concentration and evolution of Ne in an O_2-enriched bubble (Ne_b). Enrichment of other gases instead, such as N_2 or CH_4, affects Ne in an identical manner as O_2-enriched compositions, requiring greater ebullition rates to explain observed dissolved Ne concentrations in the data set.

The results of this analysis are plotted for 29 July and 26 August separately in Figure 4. Very small bubbles (<0.16 mm diameter) collapse and re-dissolve, and therefore have no effect on noble gas concentrations in the pond. The lower bound for total ebullition rates occurs when a bubble that begins as pure photosynthetic O_2 (zero concentration of the noble gases) reaches equilibrium with the surrounding water before escaping, either while on the bottom or during the bubble's rise. In this case the bubble size does not appreciably affect the ebullition rate required to explain the observed pond Ne concentrations (C_b, and thus the solution to equation (8), is nearly constant over the evaluated range of bubble sizes; see also Figure S5). Over the range of initial bubble compositions, concentrations near equilibrium are most likely in small bubbles; for example, bubbles of 0.2 mm diameter come to equilibrium with the surrounding water before reaching the surface (bubble radius of 1×10^{-4} m in Figure 4).

An extreme upper bound is a 0.5 cm diameter bubble (qualitatively as large a bubble as we saw in the pond and much larger than most bubbles we observed) which is allowed no time for equilibration before it begins to rise. Such bubbles will remain high in O_2 and contain very little noble gas. In a real environment however, it is unlikely that a bubble could grow this large prior to escaping from the pond bottom without some equilibration with the surrounding water, and this upper bound most likely overestimates ebullition for bubbles of this size.

We additionally identified a "best guess" range of bubble sizes spanning between the upper and lower bound bubble sizes and O_2-enriched composition from ~20% to 60% mole fraction O_2, covering the range of bubble compositions in the field measurements presented in Cheng et al. (2014) for a shallow, sandy marine setting with high rates of ebullition driven by photosynthesis (mean bubble size was 1 mm diameter in that study, in the middle of the best guess range presented here). The pond has a muddy bottom and likely a different primary producer community, but the choice of bubble size may still be reasonable in this setting. While most measured bubble size distributions in natural environments come from settings with ebullition of large methane bubbles (a few mm diameter; e.g. Delwiche & Hemond, 2017b), available observations suggest

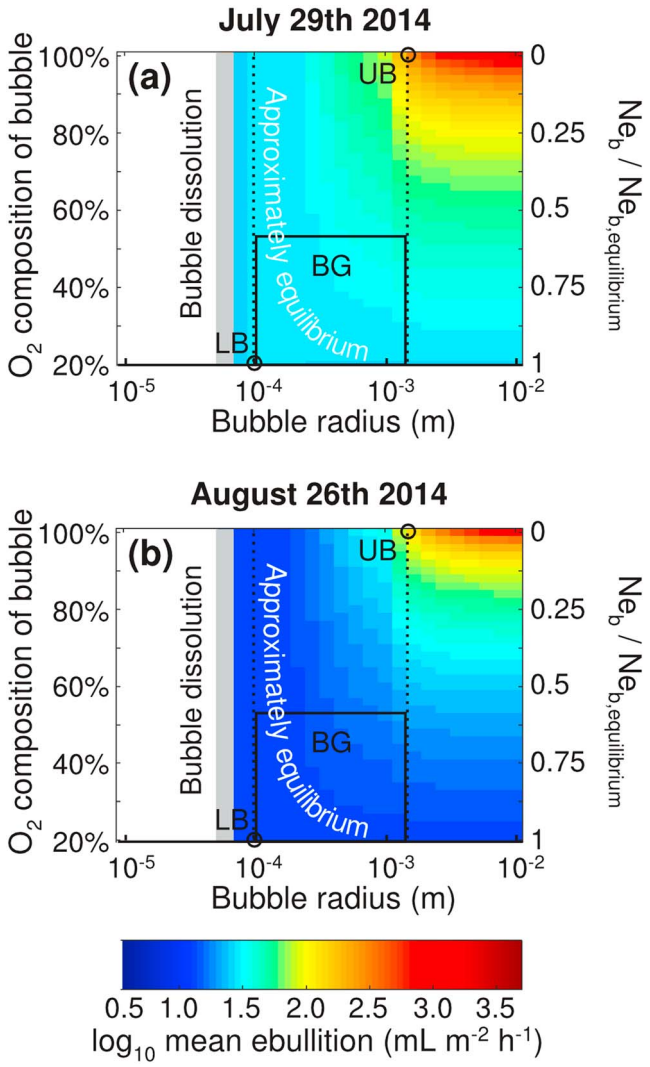

Figure 4. The mean gas ebullition rate (log-transformed) over the hours sampled on both days in this study, 09:15 to 15:45 h, over a range of assumed bubble size and initial oxygen (O_2) composition at the time the bubble begins to rise. Increasing O_2 content (left *y* axis) decreases the partial pressure of other gases—the right *y* axis is equivalently labeled as the fraction of Ne concentration in the bubble (Ne_b) compared to that expected for a bubble at equilibrium with the surrounding water for all gases (including O_2). Below an initial radius of 8×10^{-5} m (0.16 mm diameter, gray bar on plot), bubbles collapse completely before they can rise to the surface. Circles mark the lower bound (LB) and upper bound (UB) ebullition rates based on mean bubble size (dashed lines, equivalent to 0.2 mm and 0.5 cm diameter for LB and UB, respectively) and O_2 composition (equilibrium with surrounding water and 100% O_2 for LB and UB, respectively). The best guess (BG) range of O_2 composition is based on the results presented in Cheng et al. (2014).

that photosynthetic bubbles are smaller, with mean diameters of ~1 mm when generated by algae (Cheng et al., 2014) or seagrasses (Wilson et al., 2012). This range of sizes is consistent with qualitative observations of bubbles in this setting as well (Figure 3).

Over the first daytime sample period (Figure 5), including Ne-derived ebullition improved the fit of the modeled ΔAr to the measurements, leading to modeled midday data outside the uncertainty bounds of the models driven by the gas exchange parameterizations and within the uncertainty bounds of the measured saturation states. The mean ebullition rate from 9:15 to 15:45 on the first daytime period was 27(14) mL m^{-2} h^{-1} for the lower bound case (standard deviation in parentheses), 27 to 48 mL m^{-2} h^{-1} for the best guess range, and 237(121) mL m^{-2} h^{-1} for the extreme upper bound. Over the second daytime period (again 9:15 to 15:45, Figure 6), including ebullition only slightly improved the ΔAr fit; Ne-derived ebullition was roughly half that of the first day over the same hours: (13(3) mL m^{-2} h^{-1}) for the lower bound, 13 to 23 mL m^{-2} h^{-1} for the best guess range, and 110(27) mL m^{-2} h^{-1} for the upper bound. Ebullition was also apparently more evenly distributed over the sampling period without the pronounced midday peak that helped push Ar lower on the first day. This difference could be attributable to spatial and temporal heterogeneity of ebullition or could be caused by rapid equilibration between the water and atmosphere relative to the rate of ebullition.

The latter possibility points to an important caveat with this method, specifically that the noble gases may become insensitive to ebullition when diffusive gas exchange is rapid compared to the ebullition flux; that is, diffusive gas exchange can maintain Ne at atmospheric equilibrium even while ebullition is removing Ne. Noble gas derived ebullition rates and resulting fluxes should then be most sensitive when the rate of ebullition is high, diffusive gas exchange is relatively slow, and gases are undersaturated or supersaturated so that the effect of ebullition can be detected—these conditions may occur often in a shallow body of water that is rapidly heated or cooled and where wind velocities and water advection are relatively low.

Based on the biases and sensitivities of the ebullition rates evaluated for the two daytime periods, the method appears to have had an accuracy and minimum sensitivity threshold of roughly 10 mL m^{-2} h^{-1} of ebullition in this study; this was approximately the lowest value of ebullition that could be detected in the modeled versus measured Ne saturation state during either day. The best guess range of ebullition rates was similar (Figure 4). The noble gases will in general provide a lower bound for the true ebullition rate at any specific bubble size and composition. Greater sampling resolution in time and space will improve the method's accuracy.

3.4. Relationship Between Ebullition and Environmental Processes

Photosynthetic O_2 production in sunlit sediments is a likely source of ebullition. Production and respiration cause large diel changes in O_2 (10% to 150% of saturation at the sonde location, over bare sediment). O_2 is distributed heterogeneously within the pond, reflecting the spatial variability of production; a survey of O_2 around the perimeter of the study pond revealed peak O_2 of 200% to 300% of saturation in areas with visible benthic algae or vascular plants. Photosynthetic O_2 production tracks photosynthetically active radiation (PAR, 400–700 nm; Stanley & Howard, 2013; Howard, 2017), and local O_2 supersaturation may form bubbles at nucleation points (such as photosynthesizing algae).

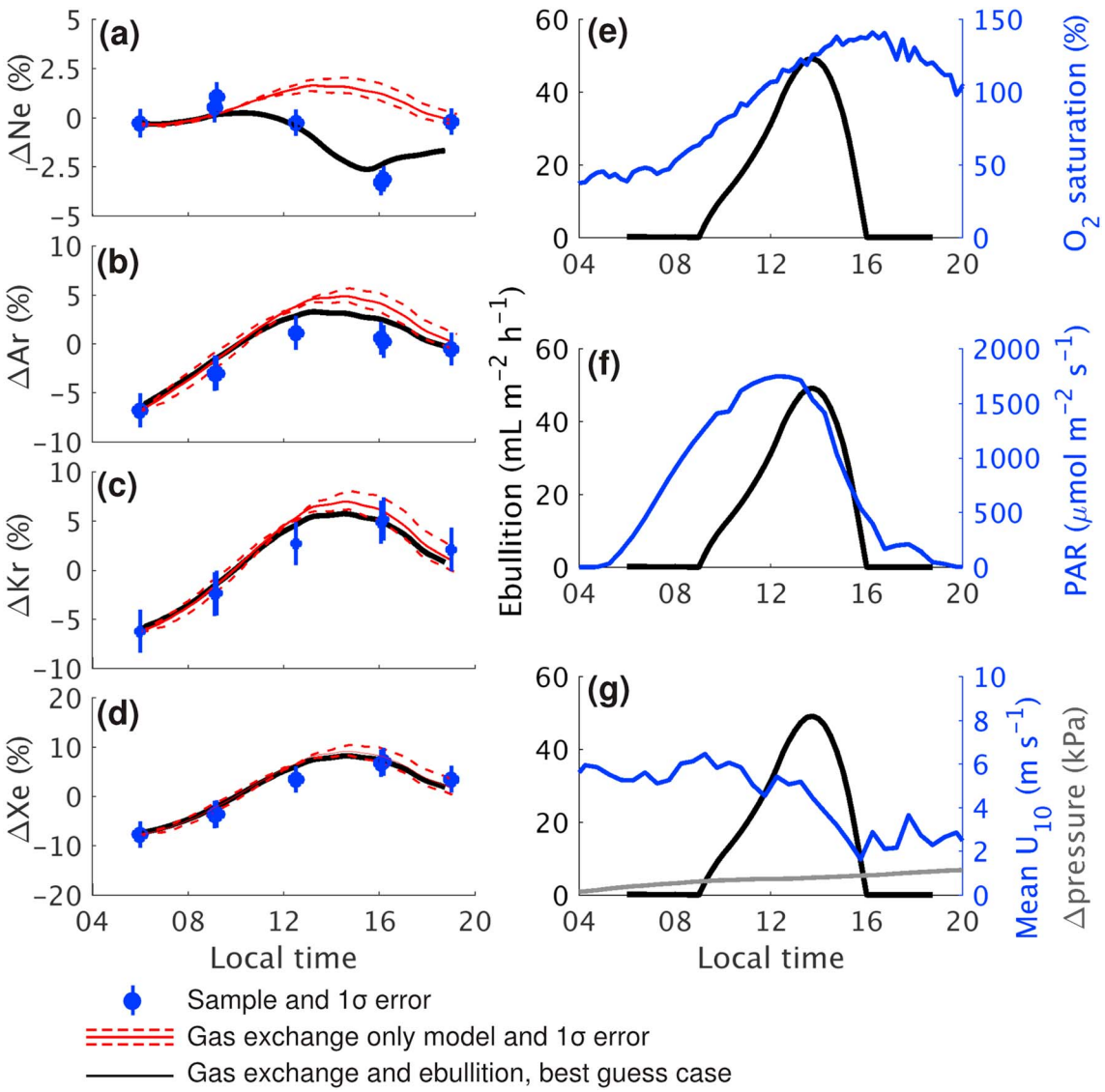

Figure 5. The saturation states of neon (ΔNe; a), argon (ΔAr; b), krypton (ΔKr; c), and xenon (ΔXe, d) on 29 July relative to in situ solubility adjusted for changes in atmospheric pressure (blue circles and one standard deviation error bars) compared to modeled saturation states using the gas exchange parameterization of Vachon and Prairie (2013) only (red line and dashed uncertainty bounds based on reported standard deviation of parameterization terms), and to gas exchange including the effects of ebullition (black solid line) derived from a Ne mass balance. The ebullition rate for 1 mm diameter bubbles with 40% initial oxygen (O_2) composition (black solid line) is plotted against environmental parameters (blue lines), including O_2 saturation state (e; plotted here as 100% at the saturation concentration expected for atmospheric equilibrium), photosynthetically active radiation flux (PAR, 400–700 nm; f), and (g) mean wind speed at 10 m (U_{10}) as well as the pressure difference from 1 atm (101.325 kPa). The lower and upper bound cases have different magnitudes of ebullition, but identical time evolution relative to the environmental parameters.

On 29 July, Ne-derived ebullition tracked the initial rise in O_2 saturation state in the water column (Figure 5). Ebullition occurred during a period of decreasing wind speed and rising atmospheric pressure and had a similar pattern to PAR (and dropped to zero concurrently with independent estimates of in situ gross photosynthetic production; Howard, 2017). On 26 August (Figure 6) the rate of ebullition was half that over the same period on 29 July and did not follow the pattern of either O_2 saturation state or PAR. In this case, peak PAR and O_2 supersaturation were slightly later in the day. At the same time, wind speed was increasing, and atmospheric pressure was 1 kPa greater than over the 29 July study period. While wind speed was similar on average over the two sample periods, higher wind speed on 29 July during the period when PAR and O_2 saturation state were increasing, compared to 26 August, may have contributed to bottom turbulence which dislodged bubbles.

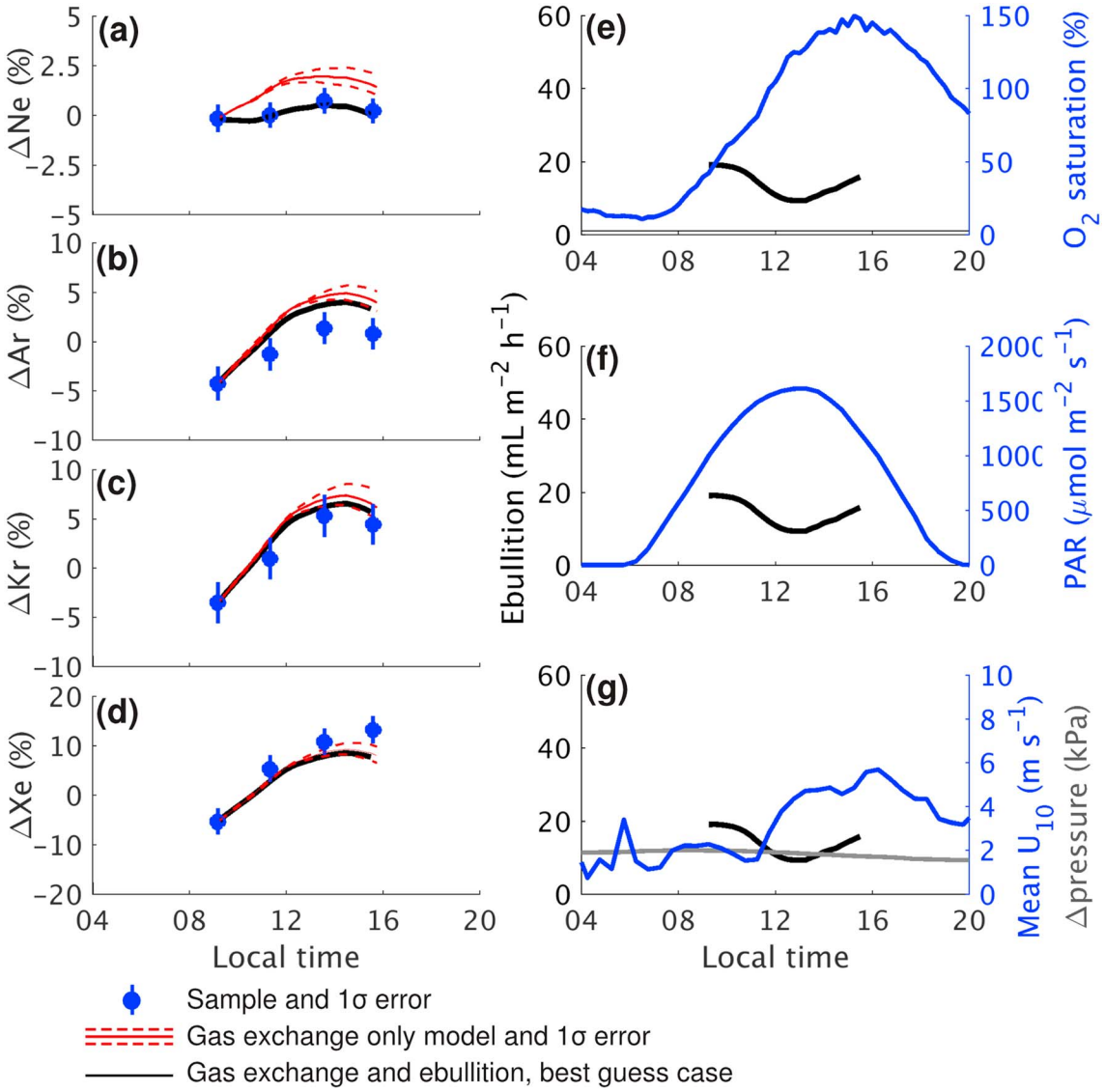

Figure 6. The saturation states of neon (ΔNe; a), argon (ΔAr; b), krypton (ΔKr; c), and xenon (ΔXe, d) on 26 August relative to in situ solubility adjusted for changes in atmospheric pressure (blue circles and one standard deviation error bars) compared to modeled saturation states from the gas exchange parameterization of Vachon and Prairie (2013) only (red line and dashed uncertainty bounds based on reported standard deviation of parameterization terms), and to gas exchange including the effects of ebullition (black solid line) derived from Ne mass balance. The ebullition rate for 1 mm diameter bubbles with 40% initial oxygen (O_2) composition (black solid line) is plotted against environmental parameters (blue lines), including O_2 saturation state (e; plotted as in Figure 5), photosynthetically active radiation flux (PAR, 400–700 nm; f), and (g) mean wind speed at 10 m (U_{10}) as well as the pressure difference from 1 atm (101.325 kPa). The lower and upper bound cases have different magnitudes of ebullition, but identical time evolution relative to the environmental parameters.

While O_2 measured at the sonde was not supersaturated over the entire period of ebullition on either day, local supersaturation at the sites of nucleation could still generate bubbles. Thus we surmise that O_2 saturation state, affected by both biological production and temperature, was related to both the timing and magnitude of ebullition. Changes in wind and pressure may also have stimulated bubble release (Maeck et al., 2014).

Continued O_2 supersaturation later on both days could have continued to generate bubbles or expanded existing bubbles. However, either Ne became insensitive to continued ebullition because of the relative rates of diffusive gas exchange and ebullition as discussed above, or ebullition slowed in the afternoon and evening. The latter might occur because either bubbles were no longer generated as PAR decreased and photosynthesis ended, or those bubbles were unable to escape the pond as easily as earlier in the day. For example, floating mats of *Ulva intestinalis* were observed in parts of the pond. *Ulva* mats have been observed in other

settings to generate oxygen bubbles which buoy the mats above the sediment (e.g. Harvey, 1858; Sundbäck & McGlathery, 2005), and in this pond we have observed them to detach from the sediments and drift onto the pond banks during periods of tidal flooding. The time-dependent production (and floatation and thus mobility) of these mats could complicate interpretation of ebullition fluxes, as bubbles generated near the top surface of these mats might escape, but those generated underneath the mats would have limited paths to the atmosphere.

Such complications may contribute to spatial and temporal heterogeneity of ebullition and its effects on dissolved gases in such environments. Future studies could make a more detailed analysis of the role of these environmental factors.

3.5. Effect of Ebullition on Production Rates

Photosynthetic O_2 escaping submerged environments via ebullition is not included in parameterizations of diffusive gas exchange fluxes. Therefore metabolism estimates from models driven by these parameterizations could underestimate O_2 efflux and thus biological production if ebullition rates are sufficiently high compared to diffusive gas exchange, leading to a heterotrophic bias in net metabolism derived from O_2.

We used the Ne-derived bubble flux to estimate the amount of photosynthetic O_2 lost through ebullition in this study as an example of the potential effect of ebullition on metabolism estimates. We calculated O_{2b} at each model time step concurrently with the noble gases, as described above, using the same best guess range of size and composition (net ebullition of O_2 over the extended bubble size and composition parameter space from Figure 4 is presented in Figure S6 in the supporting information; the true ebullition rate could be greater than the best guess range based on this range of possible parameters). Multiplying O_{2b} by the Ne-derived ebullition rate (i.e. determining the O_2-specific ebullition flux) and integrating over the entire sampling period, we found that ebullition could account for losses of -1.6 to -7.7 mmol O_2 m^{-2} for the best guess range on 29 July, integrated over the full sample period (but 98% of that production occurred over 9:15 to 15:45, the same period sampled on the second day). On 26 August, the equivalent integrated removal rate of O_2 by ebullition was -0.7 to -3.5 mmol O_2 m^{-2}.

O_2 concentrations can be evaluated using a dissolved gas mass balance, which includes an additional term for net ecosystem metabolism (NEM, also often referred to as net community production), the balance between photosynthesis and respiration. The O_2 mass balance for a tidally isolated, well-mixed environment of fixed depth is:

$$\frac{dO_2}{dt} * z * \rho = k_{O_2} * (O_{2sat} - O_2) * \rho + NEM \tag{10}$$

The same mass balance including ebullition is:

$$\frac{dO_2}{dt} * z * \rho = k_{O_2} * (O_{2sat} - O_2) * \rho + E * O_{2b} + NEM \tag{11}$$

The integrated gas exchange over each sampling period was determined from a model based on the Vachon and Prairie (2013) gas exchange parameterization, and NEM was determined by difference between the modeled gas exchange (equation (10)), or diffusive gas exchange plus ebullition (equation (11)), and the observed rate of concentration change in the water (additional details are provided in supporting information Text S5). More complex models of net metabolism are possible (Winslow et al., 2016), but this approach is adequate in order to determine the order of magnitude of ebullition relative to other fluxes of O_2.

Compared to when ebullition is neglected, NEM including ebullition integrated over the entire sampling period was 5–21% greater for the best guess range on 29 July and 1–6% greater on 26 August. Ebullition then accounted for 26–126% as much gas flux as net diffusive gas exchange alone over the sampling periods on 29 July and 3–16% as much on 26 August. Table S3 in the supporting information summarizes these fluxes, as well as the upper and lower bound cases, and the results of any particular parameter combination of bubble characteristics can be evaluated using Figure S6.

As we have no information on the actual distribution of photosynthetic bubble sizes or how they may change with time in this or similar environments, we do not explicitly calculate ebullition rates for non-

uniform bubble size distributions. However, a small number of larger bubbles can significantly increase bubble fluxes (e.g. Keeling, 1993). For example, the largest 10% of bubbles were found to account for around two-thirds of the total methane ebullition flux in a shallow montane lake (DesSontro et al., 2015). Similarly, the initial O_2 composition of the bubbles is uncertain but may be greater than assumed here; the Cheng et al. (2014) study trapped gas over a period of hours, so the resulting composition likely reflected some degree of equilibration. Future studies could better constrain the magnitude of these estimates with measurements of bubble size, or the gas composition or total volume of escaping bubbles (though ongoing equilibration of trapped gas affects estimates of the latter parameters using existing methods).

In comparison, the differences in predicted net flux of O_2 over these periods between the four gas exchange parameterizations used in this work are on the order of 25% of the integrated NEM over each day, the same order of magnitude as the effect of ebullition (at least on 29 July). These differences between the models result from the very high supersaturation of O_2 driving large diffusive gas exchange fluxes which magnify the small differences between gas exchange parameterizations. In contrast, for physicochemically similar but biologically inert Ar, neglecting ebullition introduces a systematic bias similar or greater in size than the differences between gas exchange parameterizations (a few percent), even for the lower bound ebullition case. Ebullition could then have a larger impact on (and be particularly discernable in) ratios of gases used as tracers of metabolism such as O_2/Ar (a tracer of NEM) and N_2/Ar (a tracer of denitrification) in the specific cases where bubbles are enriched in biologically produced O_2 or N_2.

Net metabolism decreases as periods of net heterotrophy are included (e.g. night). In this study pond, NEM is strongly heterotrophic throughout the summer and fall (order of -50 mmol O_2 m^{-2} day^{-1}; Howard, 2017), and including daytime ebullition of oxygen would change seasonally integrated NCP on the order of 10%. However, in settings where production and respiration are tightly coupled and NEM may be closer to zero on a daily or seasonal basis, ebullition could have a greater effect on NEM. A related consequence of bubble formation in shallow environments is that differential partitioning of O_2 and CO_2 into bubbles can lead to changes in the apparent production stoichiometry (or photosynthetic quotient) of O_2 to dissolved inorganic carbon (Howard, 2017). For example, coral reef environments are likely locations to explore for environmentally significant effects of bubble production because they can have NEM close to zero over different timescales (Albright et al., 2015; Takeshita et al., 2016) and can generate both static and rising bubbles that are highly enriched in O_2 (Bellamy & Risk, 1982; Clavier et al., 2008).

4. Conclusions

We found that four commonly used gas exchange parameterizations all did well predicting noble gas saturation states over sub-daily periods in a salt marsh pond, particularly for more soluble gases. The parameterization of Vachon and Prairie (2013) had the lowest RMSE overall. Because this parameterization is fetch dependent (unlike the other parameterizations), smaller ponds such as those abundant in salt marshes would have much lower predicted gas exchange rates using the Vachon and Prairie (2013) parameterization than using the other parameterizations.

We also demonstrated the utility of using noble gases to evaluate ebullition. Mass balances including ebullition better explained the observations than diffusive gas exchange alone. Accounting for ebullition fluxes in this setting increases O_2 production by 1–21% over daytime periods, and depending on bubble characteristics potentially more. Measurements of bubble size and composition would improve the accuracy of this technique, but noble gases add advantages of spatial integration and temporal sensitivity compared to fixed bubble traps and sensors alone.

Ebullition may be an important process to consider when using dissolved gases to study ecosystem metabolism and biogeochemical cycling in marsh ponds and potentially in other shallow aquatic environments such as sea grass beds, tidal flats, and coral reefs. The noble gases are sensitive to ebullition regardless of the source of bubbles and thus could be useful tracers for quantifying bubble fluxes of other gases such as CH_4 in such environments. The limited number of samples in this study were not sufficient to develop parameterizations of ebullition, but the recent development of field portable, low-cost mass spectrometers designed for measuring dissolved noble gases (Manning, Stanley, & Lott, 2016) promises to expand the utility of this approach.

Acknowledgments

This work would not have been possible without the outstanding logistical and in kind support of the Plum Island Ecosystems Long Term Ecological Research site and TIDE experiment staff and scientists (these projects funded by NSF OCE 1238212, NSF DEB 1354494, and Northeast Climate Science Center grant DOI G12-AC00001). We wish to thank Nancy Pau at the Parker River National Wildlife Refuge for permitting this work. All samples were collected with the assistance of Jennifer Karolewski, who was supported by the Woods Hole Oceanographic Institution (WHOI) Summer Student Fellowship program. We also wish to thank Amanda C. Spivak for the use of the water quality sonde in this study, Joshua M. Curtice, Joanne Goudreau, and William J. Jenkins at the WHOI Isotope Geochemistry Facility (http://www.whoi.edu/IGF) for feedback on sampling methods and interpretation of noble gas data, and Kimberly J. Vaeth and Philip M. Gschwend for constructive feedback in developing this manuscript. Finally, we thank the anonymous reviewers of this manuscript for greatly improving it with their thoughtful feedback. The noble gas solubilities used in this work were derived from experiments designed and conducted by Dempsey E. Lott III and William J. Jenkins as described at http://www.whoi.edu/IGF. Funding for this research was provided by NSF OCE 1233678 and the WHOI Coastal Ocean Institute. E. Howard was supported by the National Defense Science and Engineering Graduate Fellowship. The authors have no real or perceived financial or affiliation-related conflicts of interest with respect to the results of this paper. Data used in this work have been assigned a digital object identifier and are accessible through the Biological and Chemical Oceanography Data Management Office (https://www.bco-dmo.org/dataset/670694). Ancillary meteorological data are accessible from the LTER Network Information System Data Portal (Giblin & Forbirch, 2016; https://doi.org/10.6073/pasta/14eb405f583ae2384b2c6c5714776214). Additional data used in this work can be found in the tables, cited references, and in the supporting information available with the electronic version of this paper.

References

Aeschbach-Hertig, W., El-Gamal, H., Wieser, M., & Palcsu, L. (2008). Modeling excess air and degassing in groundwater by equilibrium partitioning with a gas phase. *Water Resources Research*, *44*, W08449. https://doi.org/10.1029/2007WR006454

Albright, R., Benthuysen, J., Cantin, N., Caldeira, K., & Anthony, K. (2015). Coral reef metabolism and carbon chemistry dynamics of a coral reef flat. *Geophysical Research Letters*, *42*, 3980–3988. https://doi.org/10.1002/2015GL063488

Bellamy, N., & Risk, M. J. (1982). Coral gas: Oxygen production in *Millepora* on the Great Barrier Reef. *Science*, *215*(4540), 1618–1619. https://doi.org/10.1126/science.215.4540.1618

Bieri, R. H. (1971). Dissolved noble gases in marine waters. *Earth and Planetary Science Letters*, *10*(3), 329–333. https://doi.org/10.1016/0012-821X(71)90038-0

Borges, A. V., Delille, B., Schiettecatte, L.-S., Gazeau, F., Abril, G., & Frankignoulle, M. (2004). Gas transfer velocities of CO_2 in three European estuaries (Randers Fjord, Scheldt, and Thames). *Limnology and Oceanography*, *49*(5), 1630–1641. https://doi.org/10.4319/lo.2004.49.5.1630

Brennwald, M. S., Kipfer, R., & Imboden, D. M. (2005). Release of gas bubbles from lake sediment traced by noble gas isotopes in the sediment pore water. *Earth and Planetary Sciences Letters*, *235*, 31–44. https://doi.org/10.1016/j.epsl.2005.03.004

Caffrey, J. M. (2004). Factors controlling net ecosystem metabolism in U.S. estuaries. *Estuaries*, *27*(1), 90–101. https://doi.org/10.1007/BF02803563

Cheng, C. H., Huettel, M., & Wildman, R. A. (2014). Ebullition-enhanced solute transport in coarse-grained sediments. *Limnology and Oceanography*, *59*(5), 1733–1748. https://doi.org/10.4319/lo.2014.59.5.1733

Clavier, J., Chauvaud, L., Cuet, P., Esbelin, C., Frouin, P., Taddei, D., & Thouzea, G. (2008). Diel variation of benthic respiration in a coral reef sediment (Reunion Island, Indian Ocean). *Estuarine, Coastal and Shelf Science*, *76*(2), 369–377. https://doi.org/10.1016/j.ecss.2007.07.028

Cole, J. J., Bade, D. L., Bastviken, D., Pace, M. L., & Van de Bogert, M. (2010). Multiple approaches to estimating air-water gas exchange in small lakes. *Limnology and Oceanography: Methods*, *8*(6), 285–293. https://doi.org/10.4319/lom.2010.8.285

Cole, J. J., & Caraco, N. F. (1998). Atmospheric exchange of carbon dioxide in a low-wind oligotrophic lake measured by the addition of SF6. *Limnology and Oceanography*, *43*(4), 647–656. https://doi.org/10.4319/lo.1998.43.4.0647

Crosswell, J. R. (2015). Bubble clouds in coastal waters and their role in air-water gas exchange of CO_2. *Journal of Marine Science and Engineering*, *3*(3), 866–890. https://doi.org/10.3390/jmse3030866

Crusius, J., & Wanninkhof, R. (2003). Gas transfer velocities measured at low wind speed over a lake. *Limnology and Oceanography*, *48*(3), 1010–1017. https://doi.org/10.4319/lo.2003.48.3.1010

Delwiche, K., & Hemond, H. F. (2017a). An enhanced bubble size sensor for long-term ebullition studies. *Limnology and Oceanography: Methods*, *15*(10), 821–835. https://doi.org/10.1002/lom3.10201

Delwiche, K., & Hemond, H. F. (2017b). Methane bubble size distributions, flux, and dissolution in a freshwater lake. *Environmental Science and Technology*, *51*(23), 13,733–13,739. https://doi.org/10.1021/acs.est.7b04243

DesSontro, T., McGinnis, D. F., Wehrli, B., & Ostrovsky, I. (2015). Size does matter: Importance of large bubbles and small-scale hot spots for methane transport. *Environmental Science and Technology*, *49*(3), 1268–1276. https://doi.org/10.1021/es5054286

Dugan, H. A., Woolway, R. I., Santoso, A. B., Corman, J. R., Jaimes, A., Nodine, E. R., et al. (2016). Consequences of gas flux model choice on the interpretation of metabolic balance across 15 lakes. *Inland Waters*, *6*(4), 581–592. https://doi.org/10.5268/IW-6.4.836

Forbrich, I., & Giblin, A. E. (2015). Mash-atmosphere CO_2 exchange in a New England salt marsh. *Journal of Geophysical Research: Biogeosciences*, *120*, 1825–1838. https://doi.org/10.1002/2015JG003044

Gao, Y., Lie, X., Yi, N., Wang, Y., Guo, J., Zhang, Z., & Yan, S. (2013). Estimation of N_2 and N_2O ebullition from eutrophic water using an improved bubble trap device. *Ecological Engineering*, *57*, 403–412. https://doi.org/10.1016/j.ecolend.2013.04.020

Giblin, A. E., & Forbirch, I. (2016). Eddy flux measurements during 2014 from high marsh (*Spartina patens*/short *Spartina alterniflora*) off Nelson Island Creek, Rowley, Massachusetts. Long Term Ecological Research Network dataset. https://doi.org/10.6073/pasta/14eb405f583ae2384b2c6c5714776214

Hamme, R. C., & Emerson, S. R. (2004). The solubility of neon, nitrogen and argon in distilled water and seawater. *Deep Sea Research Part I: Oceanographic Research Papers*, *51*(11), 1517–1528. https://doi.org/10.1016/j.dsr.2004.06.009

Hamme, R. C., Emerson, S. R., Severinghaus, J. P., Long, M. C., & Yashayaev, I. (2017). Using noble has measurements to derive air-sea process information and predict physical gas saturations. *Geophysical Research Letters*, *44*, 9901–9909. https://doi.org/10.1002/2017GL075123

Harvey, W. H. (1858). Nereis Boreali-Americana, or contributions to a history of the marine algae of North America: Part III, Chlorospermeae. In *Contributions to knowledge* (Vol. 10, Article 3, pp. 51–61). Washington, DC: Smithsonian Institution.

Howard, E. M. (2017). Ecosystem metabolism in salt marsh tidal creeks and ponds: Applying triple oxygen isotopes and other gas tracers to novel environments. PhD thesis, MIT/WHOI Joint Program, Feb. 2017. https://doi.org/10.1575/1912/8654

Jenkins, W. J., Lott, D. E. III, Cahill, K., Curtice, J., & Landry, P. (2010). Sampling and measuring helium isotopes and tritium in seawater. International Ocean Carbon Coordination Project Report No. 14, ICPO Publication Series 134, Sopot, Poland.

Keeling, R. F. (1993). On the role of large bubbles in air-sea gas exchange and supersaturation in the ocean. *Journal of Marine Research*, *51*(2), 237–271. https://doi.org/10.1357/0022240933223800

Komiya, S., Noborio, K., Katano, K., Pakoktom, T., Siangliw, M., & Toojinda, T. (2015). Contribution of ebullition to methane and carbon dioxide emission from water between plant rows in a tropical rice paddy field. *International Scholarly Research Notices*, *2015*, 1–8. https://doi.org/10.1155/2015/623901

Koschorreck, M., Hentschel, I., & Boehrer, B. (2017). Oxygen ebullition from lakes. *Geophysical Research Letters*, *44*, 9372–9378. https://doi.org/10.1002/2017GL074591

Kremer, J. N., Reischauer, A., & D'Avanzo, C. (2003). Estuary-specific variation in the air-water gas exchange coefficient for oxygen. *Estuaries*, *26*(4), 829–836. https://doi.org/10.1007/BF02803341

Linacre, E. T. (1993). Data-sparse estimation of lake evaporation, using a simplified Penman equation. *Agricultural and Forest Meteorology*, *64*(3-4), 237–256. https://doi.org/10.1016/0168-1923(93)90031-C

MacIntyre, S., Jonsson, A., Jansson, M., Aberg, J., Turney, D. E., & Miller, S. D. (2010). Buoyancy flux, turbulence, and the gas transfer coefficient in a stratified lake. *Geophysical Research Letters*, *37*, L24604. https://doi.org/10.1029/2010GL044164

Maeck, A., Hofmann, H., & Lorke, A. (2014). Pumping methane out of aquatic sediments; Ebullition forcing mechanisms in an impounded river. *Biogeosciences*, *11*(11), 2925–2938. https://doi.org/10.5194/bg-11-2925-2014

Manning, C. C., Stanley, R. H. R., & Lott, D. E. III (2016). Continuous measurements of dissolved Ne, Ar, Kr, and Xe ratios with a field-deployable gas equilibration mass spectrometer. *Analytical Chemistry*, *88*(6), 3040–3048. https://doi.org/10.1021/acs.analchem.5b03102

Manning, C. C., Stanley, R. H. R., Nicholson, D. P., & Squibb, M. E. (2016). Quantifying air-sea gas exchange using noble gases in a coastal upwelling zone. *IOP Conference Series: Earth and Environmental Science*, *35*, 012017. https://doi.org/10.1088/1755-1315/35/1/012017

Merlivat, L., & Memery, L. (1983). Gas exchange across an air-water interface: Experimental results and modeling of bubble contribution to transfer. *Journal of Geophysical Research*, *88*(C1), 707–724. https://doi.org/10.1029/JC088iC01p00707

Nock, W. J., Heaven, S., & Banks, C. J. (2016). Mass transfer and gas-liquid interface properties of single CO_2 bubbles rising in tap water. *Chemical Engineering Science*, *140*, 171–178. https://doi.org/10.1016/j.ces.2015.10.001

Nuttle, W. K., & Hemond, H. F. (1988). Salt marsh hydrology: Implications for biogeochemical fluxes to the atmosphere and estuaries. *Global Biogeochemical Cycles*, *2*(2), 91–114. https://doi.org/10.1029/GB002i002p00091

Park, S. H., Park, C., Lee, J.-Y., & Lee, B. (2017). A simple parameterization for the rising velocity of bubbles in a liquid pool. *Nuclear Engineering and Technology*, *49*(4), 692–699. https://doi.org/10.1016/j.net.2016.12.006

Read, J. S., Hamilton, D. P., Desai, A. R., Rose, K. C., MacIntyre, S., Lenters, J. D., et al. (2012). Lake-size dependency of wind shear and convection as controls on gas exchange. *Geophysical Research Letters*, *39*, L09405. https://doi.org/10.1029/2012GL051886

Spivak, A. C., Gosselin, K. M., Howard, E. M., Mariotti, G., Forbrich, I., Stanley, R. H. R., & Sylva, S. P. (2017). Shallow ponds are heterogeneous habitats within a temperate salt marsh ecosystem. *Journal of Geophysical Research: Biogeosciences*, *122*, 1371–1384. https://doi.org/10.1002/2017JG003780

Spivak, A. C., Gosselin, K. M., & Sylva, S. P. (2018). Shallow ponds are biogeochemically distinct habitats in salt marsh ecosystems. *Limnology and Oceanography*, *63*, 1622–1642. https://doi.org/10.1002/lno.10797

Staehr, P. A., Bade, D., Van de Bogert, M. C., Koch, G. R., Williamson, C., Hanson, P., et al. (2010). Lake metabolism and the diel oxygen technique: State of the science. *Limnology and Oceanography: Methods*, *8*(11), 628–644. https://doi.org/10.4319/lom.2010.8.0628

Stanley, R. H. R., Baschek, B., Lott, D. E. III, & Jenkins, W. J. (2009). A new automated method for measuring noble gases and their isotopic ratios in water samples. *Geochemistry, Geophysics, Geosystems*, *10*, Q05008. https://doi.org/10.1029/2009GC002429

Stanley, R. H. R., & Howard, E. M. (2013). Quantifying photosynthetic rates of microphytobenthos using the triple isotope composition of dissolved oxygen. *Limnology and Oceanography: Methods*, *11*(7), 360–373. https://doi.org/10.4319/lom.2013.11.360

Stanley, R. H. R., & Jenkins, W. J. (2013). Noble gases in seawater as tracers for physical and biogeochemical ocean processes. In P. Burnard (Ed.), *The noble gases as geochemical tracers*, *Advances in Isotope Geochemistry* (pp. 55–79). Berlin: Springer. https://doi.org/10.1007/978-3-642-28836-4_4

Stanley, R. H. R., Jenkins, W. J., Lott, D. E. III, & Doney, S. C. (2009). Noble gas constraints on air-sea gas exchange and bubble fluxes. *Journal of Geophysical Research*, *114*, C11020. https://doi.org/10.1029/2009JC005396

Stute, M., & Scholsser, P. (1993). Principles and applications of the noble gas paleothermometer. In P. K. Swart, K. C. Lohmann, J. McKenzie, & S. Savin (Eds.), *Climate change in continental isotopic records*, *Geophysical Monograph Studies* (Vol. 78, pp. 89–100). Washington, DC: American Geophysical Union. https://doi.org/10.1029/GM078p0089

Sundbäck, K., & McGlathery, K. (2005). Interactions between benthic macroalgal and microalgal mats. In E. Kristensen, R. H. Haese, & J. E. Kostka (Eds.), *Interactions between macro- and microorganisms in marine sediments*, *Coastal and Estuarine Studies* (Vol. 60, pp. 7–30). Washington, DC: American Geophysical Union. https://doi.org/10.1029/CE060p0007

Takeshita, Y., McGillis, W., Briggs, E. M., Carter, A. L., Donham, E. M., Martz, T. R., et al. (2016). Assessment of net community production and calcification of a coral reef using a boundary layer approach. *Journal of Geophysical Research: Oceans*, *121*, 5655–5671. https://doi.org/10.1002/2016JC011886

Tsai, J.-L., & Tsuang, B.-J. (2005). Aerodynamic roughness over an urban area and over two farmlands in a populated area as determined by wind profiles and surface energy flux measurements. *Agricultural and Forest Meteorology*, *132*(1-2), 154–170. https://doi.org/10.1016/j.agrformet.2005.07.008

Vachon, D., & Prairie, Y. T. (2013). The ecosystem size and shape dependence of gas transfer velocity versus wind speed relationships in lakes. *Canadian Journal of Fisheries and Aquatic Sciences*, *70*(12), 1757–1764. https://doi.org/10.1139/cjfas-2013-0241

Walmsley, J. L. (1988). On theoretical wind speed and temperature profiles over the sea with applications to data from sable island, Nova Scotia. *Atmosphere-Ocean*, *26*(2), 203–233. https://doi.org/10.1080/07055900.1988.9649300

Wanninkhof, R. (2014). Relationship between wind speed and gas exchange over the ocean revisited. *Limnology and Oceanography: Methods*, *12*. https://doi.org/10.4319/lom.2014.12.351

Weiss, R. F., & Kyser, T. K. (1978). Solubility of krypton in water and sea water. *Journal of Chemical & Engineering Data*, *23*(1), 69–72. https://doi.org/10.1021/je60076a014

Wilson, C. A., Hughes, Z. J., FitzGerald, D. M., Hopkinson, C. S., Valentine, V., & Kolker, A. S. (2014). Saltmarsh pool and tidal creek morphodynamics: Dynamic equilibrium of northern latitude saltmarshes? *Geomorphology*, *213*, 99–115. https://doi.org/10.1016/j.geomorph.2014.01.002

Wilson, C. J., Wilson, P. S., & Dunton, K. H. (2012). An acoustic investigation of seagrass photosynthesis. *Marine Biology*, *159*(10), 2311–2322. https://doi.org/10.1007/s00227-012-2016-4

Winslow, L., Zwart, J., Batt, R., Dugan, H., Woolway, R. I., Corman, J., et al. (2016). LakeMetabolizer: An R package for estimating lake metabolism from free-water oxygen using diverse statistical models. *Inland Waters*, *6*(4), 622–636. https://doi.org/10.5268/IW-6.4.883

Wood, D., & Caputi, R. (1966). *Solubilities of Kr and Xe in fresh and sea water*. San Francisco, CA: U.S. Naval Radiological Defense Laboratory.

Wunsch, C. (2006). *Discrete inverse and state estimation problems: With geophysical fluid applications*. Cambridge, UK: Cambridge University Press. https://doi.org/10.1017/CBO9780511535949

Zappa, C. J., McGillis, W. R., Raymond, P. A., Edson, J. B., Hintsa, E. J., Zemmelink, H. J., et al. (2007). Environmental turbulent mixing controls on air-water gas exchange in marine and aquatic systems. *Geophysical Research Letters*, *34*, L10601. https://doi.org/10.1029/2006GL028790